

Enhancing Multi-Text Long Video Generation Consistency without Tuning: Time-Frequency Analysis, Prompt Alignment, and Theory

Xingyao Li¹ Fengzhuo Zhang^{1*} Jiachun Pan¹ Yunlong Hou¹
Vincent Y. F. Tan¹ Zhuoran Yang^{2*}

¹National University of Singapore ²Yale University

{xingyao, fzzhang, yhou}@u.nus.edu pan.jiachun@outlook.com
vtan@nus.edu.sg zhuoran.yang@yale.edu



Figure 1: **Qualitative results for long video generation.** Applying **TiARA** to single-prompt and **TiARA+PROMPTBLEND** to multi-prompt generation on existing works yields significant improvements in the object and background consistency in the video.

Abstract

Despite the considerable progress achieved in the long video generation problem, there is still significant room to improve the consistency of the videos, particularly in terms of smoothness and transitions between scenes. We address these issues to enhance the **consistency** and **coherence** of videos generated with either single or multiple prompts. We propose the **Time-frequency based temporal Attention Reweighting Algorithm (TiARA)**, which meticulously edits the attention score matrix based on the Discrete Short-Time Fourier Transform. Our method is supported by a theoretical guarantee, the first-of-its-kind for frequency-based methods in diffusion models. For videos generated by multiple prompts, we further investigate key factors affecting prompt interpolation quality and propose **PromptBlend**, an advanced prompt interpolation pipeline. The efficacy of our proposed method is validated via extensive experimental results, exhibiting consistent and impressive improvements over baseline methods. The code will be released upon acceptance.

*Corresponding author

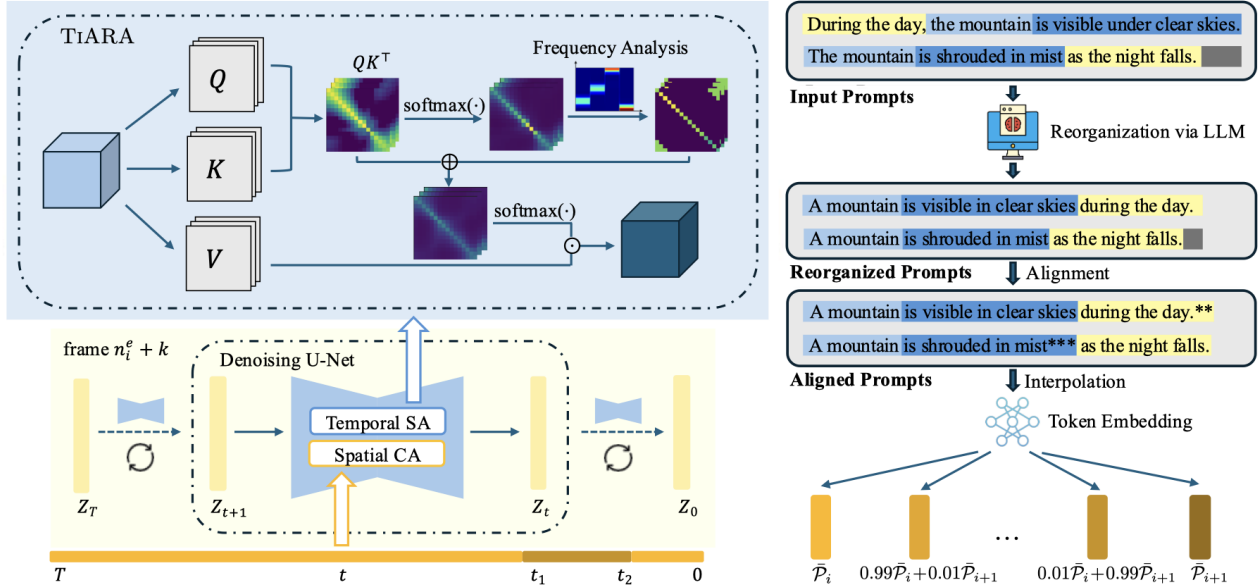


Figure 2: **The pipeline of TiARA and PromptBlend.** **Left:** To address inconsistency issues arising from excessive focus on individual frames during temporal self-attention, **TiARA** applies a reweighting matrix to the attention map at each temporal attention step in the denoising U-Net. The re-weighting values along the diagonal are selected based on the motion intensity of the generated video, determined through frequency analysis. **Right:** For multi-prompt video generation, we propose **PromptBlend** to enhance prompt interpolation. **PromptBlend** first aligns the prompts in token space and applies interpolation in token embeddings, then gradually blends the interpolated text conditioning into the inference process.

1 Introduction

Video diffusion models have achieved broad successes in many fields, including text-to-video generation [Chen et al., 2024, Guo et al., 2023], image-to-video generation [Hu, 2024], and objects animation [Blattmann et al., 2023a]. Among them, long video generation has attracted increased attention recently. Practitioners have been training more powerful video diffusion models to generate ten-second level videos with high resolutions [Zheng et al., 2024, PKU-Yuan Lab and Tuzhan AI etc., 2024].

Despite the substantial progress made in long video generation, some critical problems still persist. These problems concern the (in)consistency of long videos and, indeed, video generation with multiple prompts is poorly explored in the community. In the long videos generated by the existing methods, the number of subjects, the shape and color of the background and each single subject, and the motion pattern of the objects change abruptly and unnaturally, as shown in Fig. 1. In addition, multiple prompts are often assigned to different parts of the video. Thus, the interpolation or transition between different prompts is a critical part of the generated videos. However, existing works have not adequately investigated how to handle multiple prompt inputs to achieve better generation results.

We improve the consistency of generated long videos from two perspectives—the video hidden states and the prompt hidden states in the denoising networks as shown in Fig. 2. **First**, we introduce **Time-frequency based temporal Attention Reweighting Algorithm (TiARA)** to improve consistency by enhancing the video hidden states in the denoising network. We examine

the characteristics of temporal attention scores when the generated videos are not consistent. As shown in Fig. 3, the observed overly high values on the diagonal of the temporal attention scores inspire us to reweigh them. We assign less weight on the diagonal of the scores, encouraging the current frame to draw more information from other frames. While this reweighting method works well for videos containing slow motions, it incurs blur in the fast-moving objects due to improper smoothing on them. We resolve this problem via conducting time-frequency analysis using the Discrete Short-Time Fourier Transform (DSTFT). By identifying the motion intensity of each part in the video with DSTFT, we adaptively adjust the weight on the diagonal to remove additional blur. **Second**, we propose **PromptBlend** to improve consistency by designing the prompt hidden states in the denoising network. Our method consists of (i) prompt embedding alignment and interpolation and (ii) integration of the interpolated embeddings into the denoising network. The former involves prompt organization and token alignment. This helps to align the semantics between different prompts. Then, the interpolated embedding is applied to the denoising network according to the denoising time index and the layer index of the network. This helps to preserve the consistency of the video during the transition. We highlight that all proposed algorithms are *training-free*.

The main contributions are summarized below.

- We propose **TiARA** to improve the consistency by reweighting the temporal attention scores. **TiARA** conducts time-frequency analysis via the DSTFT to derive adaptive weights, improving the video consistency while preserving the motion in videos. **TiARA** can serve as a plug-in for existing long video generation methods. We verify its efficacy on FIFO-Diffusion [Kim et al., 2024a], Freenoise [Qiu et al., 2023], and StreamingT2V [Henschel et al., 2024]. We highlight that **TiARA** can improve the consistency in the generation of single- and multi-prompt long videos.
- We provide an accompanying theoretical analysis in addition to empirical evaluations. Frequency-based methods have been shown to be effective in various video diffusion model applications. However, all existing methods are designed based on heuristic intuitions. Our work is the *first* to provide an analysis of the frequency-based method in video diffusion model. The analysis also sheds light on the design of hyperparameters in algorithms.
- We propose **PromptBlend** to improve the consistency by designing a prompt interpolation strategy for video generation of multiple prompts. It enhances consistency by: (1) aligning semantics in different prompts before the embedding interpolation and (2) adaptively implementing the interpolated embedding according to the denoising time index and the layer index in the network. The efficacy of the overall algorithm is corroborated by extensive experiments.

2 Preliminaries

2.1 Video Diffusion Models

In video diffusion models, capturing the temporal correlation across frames is crucial for generating consistent video sequences. To address this, recent works [Blattmann et al., 2023b, Guo et al., 2023, Chen et al., 2024, Wang et al., 2023b,c] introduce additional temporal attention modules to the U-Net architecture in pretrained text-to-image models, which are

often referred to as 2D+1D U-Net. The input to U-Net is a latent $Z \in \mathbb{R}^{C \times N \times H \times W}$, where C is the channel dimension, N is the number of frames, and H and W are respectively the height and width of each frame. The newly introduced temporal attention module is implemented along the temporal axis, i.e., for any $h \in [H]$, $w \in [W]$, the input to the attention module is $Q_{h,w} = [Z_{:,1,h,w}, \dots, Z_{:,N,h,w}]^\top W_Q = Z_{:::,h,w}^\top W_Q \in \mathbb{R}^{N \times d_k}$, $K_{h,w} = Z_{:::,h,w}^\top W_K \in \mathbb{R}^{N \times d_k}$, $V_{h,w} = Z_{:::,h,w}^\top W_V \in \mathbb{R}^{N \times d_v}$, and the output of the temporal attention is

$$\text{Att}(Q_{h,w}, K_{h,w}, V_{h,w}) = \text{sm}(d_k^{-1/2} Q_{h,w} K_{h,w}^\top) V_{h,w} \quad (2.1)$$

where $\text{sm}(\cdot)$ is the row-wise softmax function, d_k and d_v are the embedding dimension of keys and values.¹ There are also some models that implement a 3D spatial-temporal attention, such as Open-Sora-Plan 1.3 [PKU-Yuan Lab and Tuzhan AI etc., 2024]. In this paper, we mainly focus on the 2D+1D U-Net, and leave the 3D structure as future work.

2.2 Long Video Generation Methods

FIFO-Diffusion and Rolling Diffusion Model Traditionally, the video frames are generated as a whole vector, where all frames share the same magnitude of noise at each denoising step. FIFO-Diffusion [Kim et al., 2024a] proposes to increase the noise magnitude of the frames according to their frame indices. In this method, all noisy frames constitute a queue. After each denoising step, the first frame in the queue is fully denoised and is popped out; and another Gaussian noise frame is appended to the queue, prepared for the next step of denoising. This method is suitable for long video generation since the first-in-first-out scheme can generate an infinite-length sequence in an autoregressive manner. A similar design is also discussed in Rolling Diffusion Model [Ruhe et al., 2024].

StreamingT2V StreamingT2V Henschel et al. [2024] extends short video generation models to long video generation using an autoregressive approach. It trains a conditional attention module that uses selected frames from the previous chunk as conditions for the current video chunk, ensuring the smoothness across chunks. An appearance preservation module is trained to incorporate anchor frame conditioning, which helps maintain consistent scenes and object features throughout generated videos.

FreeNoise FreeNoise [Qiu et al., 2023] is a training-free method for long video generation. By applying window-based attention fusion and local noise shuffling, it extends the number of frames generated at the same time and enhances temporal consistency in the output video. However, this method can only generate videos with motions of a limited scale, which is restrictive for varying contexts.

Existing problems in long video generation Although existing works propose algorithms to generate long videos, the generated videos contain inconsistent parts. As shown in Fig. 1, the baseline methods result in the number, color, and shape of objects being inconsistent across frames. We mitigate these inconsistencies.

2.3 Fourier Analysis

The Discrete Fourier Transform (DFT) and DSTFT are classical transformation methods in the frequency analysis of signals. These methods decompose a signal into a linear combination

¹For simplicity, we omit the $\sqrt{d_k}$ in (2.1) throughout the paper.

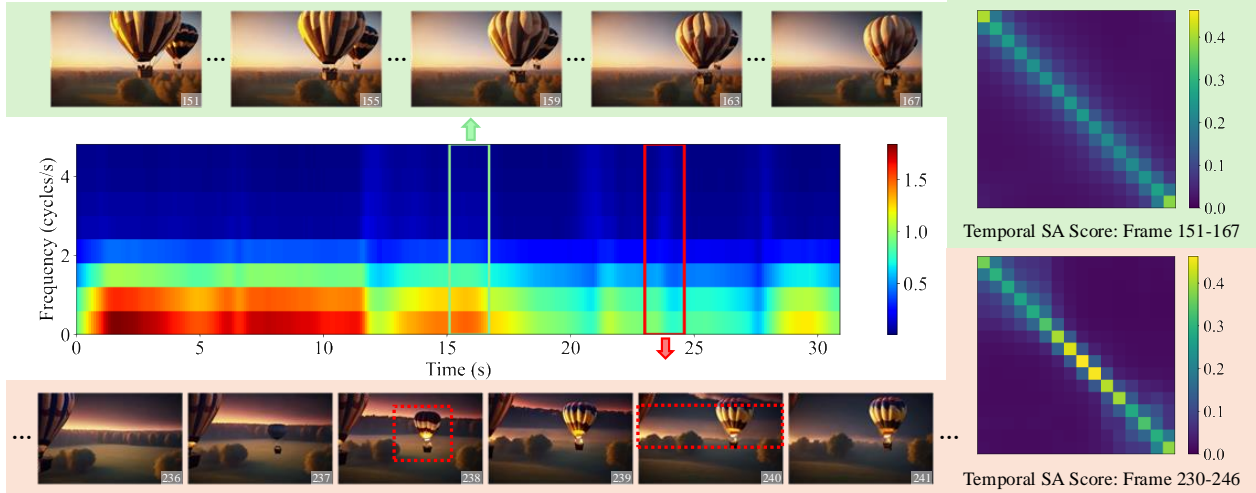


Figure 3: **Analysis of motion and temporal attention maps.** We analyze two segments within a 310-frame video. **Left:** The segment outlined in green represents a well-generated sequence with active motions. The segment outlined in red contains poorly generated content between frames 236 and 241, with inconsistent areas marked by red dotted boxes within certain frames. **Right:** The corresponding averaged temporal attention scores for these two segments. For the poorly generated frames, the attention values along the diagonal are significantly higher.

of orthogonal trigonometric basis functions. The DFT of a discrete-time signal $x : [N] \rightarrow \mathbb{R}$ with length N is defined as $\text{DFT}(x, k) = \sum_{n=0}^{N-1} x_n e^{-i\frac{2\pi kn}{N}}$ for all $k \in [N]$. Here the DFT of x at frequency k is a function of the *global* information of the signal. However, in various scenarios, the properties of signals change dynamically across time [Griffin and Lim, 1984, Durak and Arikan, 2003]. For example, in an audio signal of the enunciation of the sentence, each word has its own frequency characteristics. In these cases, it is more appropriate to analyze the frequency characteristics of *local* parts of the signal. The DSTFT achieves this goal using a *window* function $\psi : [N] \rightarrow \mathbb{R}$ and $\text{DSTFT}(x, \psi, m, k) = \sum_{n=0}^{N-1} x_n \psi_{n-m} e^{-i\frac{2\pi kn}{N}}$, for all $k, m \in [N]$. Common choices include the Hann window and the Gaussian window [Barros and Diego, 2005, Janssen, 1991]. We denote the size of the support of ψ as L . The support and the value of the window at position m mitigate the influence from the signals outside the window on this “local” frequency. Due to the periodicity of $e^{-i\frac{2\pi kn}{N}}$ for k , the frequency k near 0 or N is low frequency, and the value near $N/2$ is high frequency. This inherent periodicity of DFT and DSTFT also extends the value of x_n to n beyond $[N]$, i.e., $x_n = x_{n \bmod N}$ for all $n \in \mathbb{Z}$. In the following, we use this extended version of all the quantities related to the sequence length N .

3 Methods

In Section 3.1, we examine the temporal attention scores of inconsistent frames in generated long videos and propose a temporal attention reweighting method based on our findings. In Section 3.2, we analyze the limitations of this method and enhance it with time-frequency analysis. In Section 3.3, we propose a new effective prompt interpolation method.

3.1 Temporal Attention Reweighting

Observations from Temporal Self Attention As mentioned in Section 2.2, generated long videos often exhibit frame-to-frame inconsistencies. Here, we examine the frequency characteristics of these inconsistencies and delve into the denoising networks to explore intermediate variables correlated with them. In the 2D+1D structure introduced in Section 2.1, the temporal attention plays a critical role in capturing the correlation across frames. Thus, we analyze the attention scores of the temporal attention modules in consistent and inconsistent part of the generated videos.

We adopt a 310-frame video clip generated using FIFO-Diffusion [Kim et al., 2024a] as a representative example. As shown in Fig. 3, the video displays sudden appearances of objects and abrupt scene changes in some frames. We apply DSTFT to the video to analyze the signal in the frequency domain, and examine the temporal attention scores during generation. We make the following observations: (1) The inconsistent part has substantially more power at the highest few frequencies bands in its DSTFT spectrum. In contrast, the power of the consistent part concentrates on relatively low-frequency part of the spectrum. (2) The temporal attention scores disproportionately concentrate along the diagonal for the inconsistent generated frames, unlike that in the consistent frames. This suggests that an excessive focus on the diagonal in the temporal attention can be a contributing factor to these inconsistencies.

The first observation motivates us to define the power of the inconsistent part of the video as a function of the spectrum that at frequencies higher than a certain threshold k_t in our theoretical analysis (Section 4). The second observation dovetails with our intuition. Namely, when the temporal attention scores along the diagonal are higher, frames gather less information from other frames, which further results in increased inconsistency and reduced smoothness in the generated video.

Temporal Attention Reweighting Based on the above observations, we propose a temporal attention reweighting method to enhance the consistency of the generated videos.

We define the reweighting matrix as $\Lambda = -\alpha \cdot I_{N \times N} \in \mathbb{R}^{N \times N}$, where $\alpha \geq 0$. This matrix is applied to the correlation matrix before the softmax operation in (2.1), adjusting the attention distribution to reduce over-concentration on the diagonal and improve temporal consistency, i.e., $\overline{\text{Att}}(Q, K, V) = \text{sm}(QK^\top + \Lambda)V = \bar{A}V$. By subtracting a positive value from these diagonal entries, we encourage each frame to draw more information from other frames and maintain stronger correlations with them, thereby achieving greater consistency and smoothness between frames. Additionally, the reweighting value can be further optimized to balance between content consistency and dynamic intensity of the video.

It is also worth noting that in video generation, particularly for long videos, it is desirable for the frame to have more correlation with its neighbouring frames rather than distant frames. To achieve this, we also apply a reweighting procedure on the lower-left and upper-right corner of temporal attention maps.

3.2 TiARA

While temporal attention reweighting can effectively improve the consistency of generated videos, this technique is less suitable for video clips containing intense movements. In these cases, the weight matrix Λ will “over-smooth” the frames along the time axis, leading to blurring artifacts. As illustrated in Fig. 4, this original video generated from FIFO-Diffusion



Figure 4: **Qualitative comparison of reweighting schemes.** We compare the original FIFO (Top) with its augmented versions: with temporal attention reweighting only (Middle) and with motion intensity adjusted reweighting, referred to as **TiARA** (Bottom). The top row shows flag color inconsistencies, the middle row has blurred flag edges, while the bottom row maintains clarity and consistency.

becomes inconsistent after several frames, where the color and shape of the rainbow flag changes. With the reweighting scheme applied to the temporal attention, the generated video is indeed consistent in its color but gets blurry along the edges of the flag. This occurs because the edges of the flag involve a series of high-frequency movements, which are over-smoothed by the weight matrix Λ over time.

To address this issue, we introduce a time-frequency analysis approach that enables us to dynamically adjust the application of temporal attention reweighting. By analyzing the temporal signal in the Fourier domain, we can identify motion intensity and set different values along the diagonal of the reweighting matrix Λ . Concretely, in regions with slow motions, we assign a smaller (i.e., more negative) value to $\Lambda_{i,i}$ to encourage each frame to incorporate more information from its neighboring frames. In contrast, in areas with intense motions, we set $\Lambda_{i,i}$ closer to zero, allowing the frames to prioritize their own features. This dynamic approach preserves the intense motions in active regions while maintaining consistency in other parts.

The temporal attention scores reflect the correlation between a frame and other frames, capturing information about movements. Therefore, in order to estimate the motion intensity, we use DSTFT on each row of the normalized attention map $A = \text{sm}(Q_{h,w}K_{h,w}^\top)$. The window ψ in DSTFT helps to extract the local motion intensity of the video instead of the averaged motion intensity over the whole video. By setting a threshold for the high/low motion frequencies, we obtain a high-frequency percentage of the motion signal, which we denote as *motion intensity* ρ . The motion intensity ρ_i of the i -th frame is defined as

$$\rho_i := \frac{\sum_{\phi_1 \leq k < \phi_2} |\text{DSTFT}(A_{i,:}, \psi, i, k)|^2}{\sum_{k < \phi_2} |\text{DSTFT}(A_{i,:}, \psi, i, k)|^2}, \quad (3.1)$$

where ϕ_1 is a threshold separating the high frequency motion from the low frequency motion and ϕ_2 is a threshold between the high frequency motion and abnormal motion. The reweighting value Λ should be negatively correlated with the motion intensity. In our method, we chose the relation to be linear, i.e., $\Lambda_{i,i} = -\alpha(1 - \rho_i)$. The full pseudocode of our dynamic temporal attention reweighting method, **Time-frequency based temporal Attention Reweighting Algorithm (TiARA)**, is presented in Algorithm 1. These procedures correspond to Lines 6 and 7 of Algorithm 1. We further elaborate on several details of Algorithm 1. First, as noted

Algorithm 1 TIARA

```
1: Input: Queries  $\{Q_{h,w}\}_{h,w=1}^{H,W}$ , Keys  $\{K_{h,w}\}_{h,w=1}^{H,W}$ , Values  $\{V_{h,w}\}_{h,w=1}^{H,W}$ , thresholds  $\phi_1, \phi_2$ ,  
   reweighting coefficient  $\alpha$ , base weight matrix  $\Lambda \in \mathbb{R}^{N \times N}$ .  
2: for  $h \in [H]$ ,  $w \in [W]$  do  
3:    $A \leftarrow \text{sm}(Q_{h,w}K_{h,w}^\top)$ ,  $\lambda \leftarrow []$   
4:   for  $i$  in  $1, \dots, N$  do  
5:      $\tilde{A}_{i,:} \leftarrow \text{Pad}(A_{i,:}, \lfloor \frac{L}{2} \rfloor, \lfloor \frac{L}{2} \rfloor)$   
6:     Update  $\rho_i$  as in (3.1) with  $\tilde{A}_{i,:}$   
7:      $\lambda.\text{append}(-\alpha(1 - \rho_i))$   
8:   end for  
9:    $\text{diag}(\Lambda) \leftarrow \lambda$ ,  $Z_{h,w} \leftarrow \text{sm}(Q_{h,w}K_{h,w}^\top + \Lambda)V_{h,w}$   
10: end for  
11: Return  $\{Z_{h,w}\}_{h,w=1}^{H,W}$ 
```

in Section 3.1, the reweighting on the lower-left and the upper-right corner of the attention score is included in the base weight matrix Λ as the input. We only modify the diagonal of Λ according to the motion intensity. Second, for the boundary frames, we pad the attention scores in Line 5 for plausible DSTFT result. We adopt periodic padding in the experiments.

3.3 Multi-Prompts Alignment and Interpolation

In real-world applications, generating a complete long video often requires multiple prompts. The interpolation or transition between different prompts strongly influences the consistency of the generated videos. Some works have conducted preliminary explorations on this topic, e.g., Gen-L-Video [Wang et al., 2023a], FIFO-Diffusion [Kim et al., 2024a], and MVTG [Oh et al., 2023] propose switching directly from one prompt to the next during video generation, resulting in noticeable inconsistencies between scenes. An example of inconsistency is shown in Fig. 1, where new mountains appear and grow unrealistically during the transition between prompts. In FreeNoise Qiu et al. [2023], a motion injection method is introduced to control the inconsistency between two prompts. However, this method is restrictive because it can only deal with changes in motion verbs and it can only work on a limited motion scale.

We propose PROMPTBLEND, an effective pipeline for multi-prompt transitions. The pipeline is shown in Fig. 2, and the pseudo code is provided in Appendix A. **First**, the components of each input prompt are organized in a prescribed order, i.e., [*The subject*] [*is doing something*] [*at some time*] [*in some place*]. This operation can be carried out by the in-context learning of large language models [Dong et al., 2022]. The prompt template is provided in Appendix H. **Then**, to align the prompts in token space, we equalize component lengths in each prompt by padding extra tokens for shorter component instances. Instead of using blank tokens for padding, we repeat tokens of the shorter instance until it shares the same length as the longest instance across prompts. These two procedures derive the aligned prompt embeddings $\{\tilde{\mathcal{P}}_i\}_{i=1}^m$, and we then clarify how to use these embeddings as text conditioning during video generation.

Assume the total generated frames are divided into segments, marked with the starting and ending frame of prompt i : $\{(n_i^s, n_i^e)\}_{i=1}^m$, where indices of the transition frames are between n_i^e and n_{i+1}^s . For the non-transition frames between n_i^s and n_i^e , we adopt the i -th prompt $\mathcal{E}(\tilde{\mathcal{P}}_i)$ as the text conditioning for the U-Net, where \mathcal{E} represents the text encoder. For frame n in



Figure 5: **Qualitative comparison between Motion Injection (MI) and Prompt Blend (PB)**. Motion Injection fails to capture the semantics of the second prompt in both cases, while PROMPTBLEND successfully generates both prompts with greater consistency.

the transition window $[n_i^e, n_{i+1}^s]$, we obtain the text conditioning $\mathcal{E}(\mathcal{P}_C)$ for the cross attention blocks at denoising time step t and U-Net layer d as follow:

$$\mathcal{P}_C(n, t, d) = \begin{cases} (1-a_n)\bar{\mathcal{P}}_i + a_n\bar{\mathcal{P}}_{i+1} & t \in [t_1, t_2] \text{ or } d \geq D \\ \bar{\mathcal{P}}_i & \text{otherwise} \end{cases}$$

where $a_n = (n - n_i^e)/(n_{i+1}^s - n_i^e) \in [0, 1]$. In practice, $[t_1, t_2]$ is set to be an interval located at the later phase of the denoising process, and D is a prescribed layer index threshold, with $d \geq D$ indicating the decoder part in the U-Net. The design of this interpolation scheme is built upon two previous findings: (1) Prompt instruction at later denoising steps (i.e., $t \in [t_1, t_2]$) primarily influence the generation of object shapes [Qiu et al., 2023, Balaji et al., 2022, Cao et al., 2023, Liew et al., 2022]. (2) The decoder part of the denoising U-Net (i.e., $d \geq D$) mainly influence the semantic details [Qiu et al., 2023] while preserving the scene layout [Cao et al., 2023]. Thus, our interpolation scheme can gradually introduce elements of the next prompt to the video, and is less likely to result in inconsistencies.

Comparison to Motion Injection in FreeNoise FreeNoise [Qiu et al., 2023] introduces Motion Injection that incorporates an interpolated prompt at later denoising time steps and U-Net decoders within the transition window. After the transition window, Motion Injection continues to apply the first prompt for the non-decoder components and across most time steps. In contrast, our interpolation scheme transitions completely to the subsequent prompt after the transition window $[n_i^e, n_{i+1}^s]$.

Motion Injection facilitates a smoother, motion-focused transition within a *single* scene, as the overall structure generation remains conditioned on the initial prompt throughout. However, this approach is restricted to transitions between motions and has limited applicability for diverse scene changes. By introducing prompt alignment method, our design maintains component consistency during interpolation without depending on the first prompt. Consequently, PROMPTBLEND adapts seamlessly to multiple prompts, allowing for consistent video generation across *multiple* consecutive scenes. Experimental comparison results are shown in Fig. 5.

4 Theoretical Analysis

For the theoretical analysis, we consider the case where the value V is the concatenation of bounded scalars, i.e., $d_v = 1$, and $|v_i| \leq B_V$ for all $i \in [N]$. The results for $d_v > 1$ can be easily

derived by considering each dimension of V . To highlight the main intuitions behind T1ARA, we consider a simplification of it as follows:

$$x = \text{sm}(QK^\top)V = A^X \cdot v, \quad (4.1)$$

$$y = \text{sm}(QK^\top - \alpha \cdot I_{N \times N})V = A^Y \cdot v, \quad (4.2)$$

where A^X and A^Y are the attention scores of the original and improved temporal attention, respectively. The weights for all the time steps share the same value. We also simplify the weight matrix Λ to be diagonal.

Performance metric Inconsistency in videos usually manifests as unnatural high-frequency changes in the frames across time, as shown in Fig. 3 and Section 3.1. For a pixel that varies across time, also called a *signal* x , we define the *inconsistency error* of a signal x in a local neighborhood of time τ as $E(x, \tau) := \sum_{k=k_t}^{\lfloor N/2 \rfloor} |\text{DSTFT}(x, \psi, \tau, k)|$, where $|z|$ represents the magnitude of the complex number z , and $0 < k_t \leq \lfloor N/2 \rfloor$ is the threshold of the frequency index to distinguish the inconsistent part of the video. ϕ_2 in T1ARA is an estimate of this value. For example, this can be set to $5 \cdot 2\pi/N$ in Fig. 3. The metric $E(x, \tau)$ serves as a quantification of the signal that originates from rapid and unnatural motion in the video.

To facilitate our theoretical analyses, we make three assumptions.

Assumption 4.1 (Existence of inconsistency). The original signal $x = x^{(N)}$ of length N contains non-negligible inconsistency error. More precisely, there exists a constant $C > 0$ (not dependent on τ) such that $\liminf_{N \rightarrow \infty} E(x^{(N)}, \tau) \geq C$ for all $\tau \in \mathbb{Z}$.

This assumption states that there is a non-negligible inconsistency error in the original output of the temporal attention. Under this case, we will show that T1ARA decreases $E(y, \tau)$. We assume that such inconsistency appears in each time step $\tau \in [N]$ for the ease of analysis. Our results can be easily generalized to the situation where the inconsistency only appears in a strict subset of timesteps $N_{\text{inconsistent}} \subseteq [N]$.

Assumption 4.2 (Approximate time-homogeneity). The attention scores are approximately time-homogeneous, i.e., there exists a constant $\gamma > 4$ such that

$$|A_{i,i+k}^X - A_{j,j+k}^X| = O(N^{-\gamma}) \text{ for all } i, j, k \in \mathbb{Z}.$$

This assumption states that the attention scores at different time steps are approximately homogeneous. This can be empirically observed as the similar pattern of attention scores in each row in Figure. 3. We note that the indexes $i, j, i+k$, and $j+k$ do not have to belong to the discrete interval $[N]$. If they do not lie in $[N]$, we periodically extend of A which originates from DSTFT and is defined in Section 2.3. This assumption states that the attention scores at different time steps are approximately homogeneous. For example, this assumption is satisfied when the queries and keys satisfy $q_i^\top k_j = \exp(-|i-j|)$ for all $i, j \in \mathbb{Z}$, where $|i-j|$ denotes the difference between i and j modulo N . This type of homogeneity assumption has also been adopted in the existing works to analyze the properties of transformers [Dong et al., 2021].

As discussed in Section 3.1, the large values in the diagonal of the attention score A^X contribute to the inconsistency of the video. This motivates us to define the dynamic component of A^X by setting the diagonal components to zeros, i.e., $A_{i,j}^{X,\text{dyn}} = A_{i,j}^X$ for $i \neq j$, and $A_{i,i}^{X,\text{dyn}} = 0$. The corresponding output is then denoted as $x^{\text{dyn}} = A^{X,\text{dyn}} \cdot v$. We respectively term $A^{X,\text{dyn}}$ and x^{dyn} as the dynamic components of A^X and x , since $A^{X,\text{dyn}}$ and x^{dyn} represent how all the other frames influence the value of the current frame. This corresponds to the *dynamics* of the video.

Table 1: **Quantitative results on Single- (S) and Multi- (M) prompt generation in FIFO, StreamingT2V (ST2V) and FreeNoise.** In single-prompt case, ‘‘Ours’’ refers to TIARA and for multi-prompt case, ‘‘Ours’’ refers to both TIARA and PROMPTBLEND.

	SC (\uparrow)	BC (\uparrow)	TF (\uparrow)	MS (\uparrow)	CTS (\uparrow)	WE (\downarrow)
FIFO (S)	92.38	94.55	94.24	96.48	99.72	0.0258
FIFO + Ours (S)	94.13	95.16	96.85	98.10	99.87	0.0102
ST2V (S)	91.08	95.57	97.33	98.13	98.67	0.0108
ST2V + Ours (S)	92.95	96.41	98.09	98.79	98.82	0.0056
FreeNoise (S)	95.48	97.42	96.50	97.46	99.87	0.0135
FreeNoise + Ours (S)	98.35	98.64	97.35	97.90	99.91	0.0076
FIFO (M)	85.25	90.66	95.83	97.63	99.78	0.0115
FIFO + Ours (M)	88.87	92.43	97.68	98.66	99.89	0.0039

Assumption 4.3 (Separation between dynamic and inconsistency). For the frequencies that contribute to the inconsistency error, the low-frequency part x^{dyn} has strictly less power than x , i.e., for all $\tau \in [N]$, and $k_i \leq k \leq \lfloor N/2 \rfloor$, we have that $|\text{DSTFT}(x^{\text{dyn}}, \psi, \tau, k)| \leq \kappa \cdot |\text{DSTFT}(x, \psi, \tau, k)|$ for $\kappa < 1 - \min_{i \in [N]} A_{i,i}^X$.

This assumption mainly states that the inconsistency of the dynamic part is strictly less than that of the whole video. This assumption holds in a wide range of realistic applications since smooth and consistent videos usually have small values in the high-frequency components of DSTFT. This assumption can also be term as the ‘‘separation’’ between the dynamic and inconsistent parts since the coefficient κ is strictly less than 1. Usually, the amplitudes of DSTFT of the dynamic and smooth videos are stable, and we can roughly regard this as a constant. Then a larger κ implies that the DSTFT of the video $\text{DSTFT}(x, \psi, \tau, k)$ has a smaller amplitude at high frequency, since $|\text{DSTFT}(x, \psi, \tau, k)| = |\text{DSTFT}(x^{\text{dyn}}, \psi, \tau, k)|/\kappa$. Equipped with the above assumptions, we state our main performance guarantee as follows.

Theorem 4.4. Under the above assumptions, for any $\eta \in [\kappa/(1 - \min_{i \in [N]} A_{i,i}^X), 1)$, there exists an α (see (4.2)) that depends on κ , η , and A^X , such that the inconsistency in $y = y^{(N)}$ satisfies $\limsup_{N \rightarrow \infty} \frac{\mathbb{E}(y, \tau)}{\mathbb{E}(x, \tau)} \leq \eta$ for all τ .

The proof of Theorem 4.4 is provided in Appendix E. This result states that the inconsistency in the original signal x can be reduced by the simple algorithm in (4.2) with a proper choice of α . In the proof, we choose $\alpha = \log(1 + (1 - \eta)/(\eta(1 - \min_i A_{i,i}^X - \kappa)))$. A smaller value of κ yields a larger value of α . We deduce that it is appropriate to choose a larger α if $|\text{DSTFT}(x, \psi, \tau, k)|$ has smaller amplitudes at higher frequencies. In Section 3.2, we adhere to this intuition, where we choose $\Lambda_{i,i}$ according to $|\text{DSTFT}(A_{i,i}^X, \psi, \tau, k)|$. The reason to use $\text{DSTFT}(A_{i,i}^X, \psi, \tau, k)$ instead of $\text{DSTFT}(x, \psi, \tau, k)$ is that some videos deviate from being approximately homogeneous, and we would like to distinguish between the local frequencies at each time step.

5 Experiments

5.1 Experimental Setting

Implementation details We implement our methods on three long video generation models: FIFO-Diffusion [Kim et al., 2024a], (referred to as FIFO for simplicity) FreeNoise [Qiu et al.,

Table 2: Ablation study on reweighting scheme for single-prompt generation with FIFO.

	SC (\uparrow)	BC (\uparrow)	TF (\uparrow)	MS (\uparrow)	CTS (\uparrow)	WE (\downarrow)
Original	92.38	94.55	94.24	96.48	99.72	0.0258
Corner reweighting	92.89	94.80	94.74	96.66	99.74	0.0239
Diag reweighting	93.57	95.04	96.46	97.99	99.85	0.0107
TiARA	94.13	95.16	96.85	98.10	99.87	0.0102

2023] and StreamingT2V [Henschel et al., 2024]. Videos of 64 frames are generated for single prompt inputs. For multi-prompt, we generate 310 frames using two prompts for each video with 100 transition frames. The reweighting value α is adjusted between 5 and 7. For DSTFT, we use the Blackman Window with window length $L \in \{7, 8, 9\}$. ChatGPT [Achiam et al., 2023] is adopted for the organization of multiple prompts.

Prompts We use 34 prompts for single prompt generation, and 13 sets of prompts for multi-prompt generation. The prompts are designed to cover commonly used scenarios. Some of single prompts are sourced from prompt list provided by [Henschel et al., 2024], while all multi-prompts are created by ourselves. The prompts are listed in Appendix I.

Evaluation metrics For evaluation of the generated videos, we select several metrics from VBench [Huang et al., 2024] and EvalCrafter [Liu et al., 2024], including Subject Consistency (SC), Background Consistency (BC), Temporal Flickering (TF), Motion Smoothness (MS), Warping Error (WE) and CLIP-Temp Score (CTS). Detailed explanations of these evaluation metrics are provided in the Appendix F.

5.2 Experimental Results

Qualitative results for single-prompt and multi-prompt generation are illustrated in Fig. 1, with additional results provided in Appendix J. Quantitative results are presented in Table 1. For single prompt video generation, the result indicates that **TiARA** significantly enhances the content consistency and temporal quality of the base models. Specifically, the improved SC, BC, and CTS imply that videos generated with **TiARA** enjoy greater visual and semantic consistency. Moreover, the reduced TF, WE and the increased MS underscore the effectiveness of **TiARA** in improving the temporal quality of generated videos. For multi-prompt generation, the integrated method, **TiARA+PROMPTBLEND**, achieves even greater gains in SC and BC compared to the base model, further showcasing its effectiveness in complex generation scenarios. We also conducted a user study to evaluate the generated single-prompt and multi-prompt videos based on human preferences. The results, shown in Fig. 6, indicate a strong preference for videos generated with our method over those generated without it, illustrating its impact on user-perceived quality. The details of user study setup are postponed to Appendix F.

We also compare the improvement of **PROMPTBLEND** over the Motion Injection method in FreeNoise [Qiu et al., 2023] in Fig. 5. Each generated videos have 310 frames, with text conditioning transitioning from the first prompt to the second prompt between frame 50 and 150, which gives sufficient length for generating the second prompt. In both cases, Motion Injection fails to generate the second prompt, whereas **PROMPTBLEND** successfully generates both prompts while maintaining content consistency.

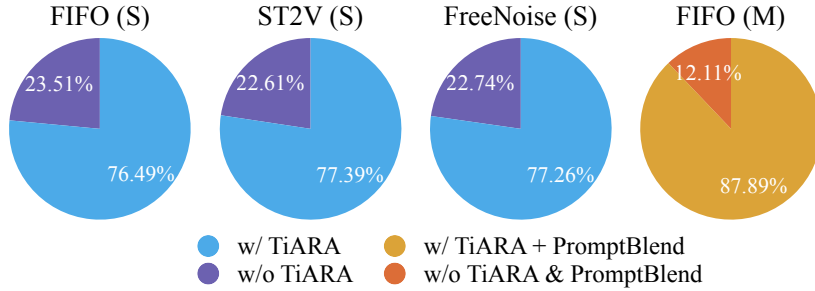


Figure 6: **User studies.** User preference ratio on Single- (S) and Multi- (M) prompt generation in FIFO, ST2V and FreeNoise.

Table 3: **Ablation study on PromptBlend for multi-prompt generation with FIFO.**

	SC (\uparrow)	BC (\uparrow)	MS (\uparrow)
Original	85.25	90.66	97.63
Aligned	85.74	91.17	97.71
Aligned + Interp	85.98	91.27	97.71
PromptBlend	86.52	91.36	97.73

5.3 Ablation Study

In this section, we present several quantitative and qualitative experiments to evaluate the effectiveness of `TiARA` and `PromptBlend`. First, we conduct an ablation study on each component of `TiARA` in the context of single-prompt video generation. Four cases are tested: (1) the original FIFO; (2) reweighting applied only to the lower-left and upper-right corners of the temporal attention map; (3) reweighting applied only to the diagonal entries of the temporal attention map; and (4) `TiARA` with both reweightings. The results, shown in Table 2, indicate that applying reweighting to the corners alone provides a modest improvement, while reweighting along the diagonals yields better performance. The best results are achieved with combined reweightings, highlighting the importance of each component in `TiARA`. We also qualitatively show the efficacy of `TiARA` compared to the reweighting without time-frequency analysis in Fig. 4.

In Table 3, we evaluate the improvements achieved by our prompt alignment and interpolation methods individually in the multi-prompt video generation task. The comparison is conducted on multi-prompt FIFO across four types of text conditioning schemes: (1) original prompt inputs; (2) prompts aligned using our method; (3) aligned and interpolated prompts applied as text conditioning for all layers and time steps; and (4) `PromptBlend`. The performance gap between (1) and (2) demonstrates the effectiveness of our prompt alignment strategy, with significant improvements in SC, BC, and MS for videos generated using aligned prompts. Comparing (2) and (3) confirms that our interpolation scheme further enhances performance beyond simply using interpolated prompts as conditioning for all layers and time steps, with both approaches outperforming the no-interpolation schemes. An ablation study on the influence of prompt alignment on prompt interpolation can be found in Appendix G. The related works and limitations are included in Appendix B and Appendix C.

6 Conclusion

In this paper, we uncover the relationship between temporal attention scores and the consistency and smoothness of generated videos. Building on this insight, we introduce TIARA, which enhances consistency in long video generation. We also theoretically demonstrate its effectiveness under reasonable assumptions. Additionally, we propose PROMPTBLEND, a technique for smoothly interpolating between prompts to improve consistency in multi-prompt video generation. Extensive quantitative and qualitative experiments across various long video generation pipelines and text prompts confirm the effectiveness of both TIARA and PROMPTBLEND in enhancing video consistency.

References

- J. Achiam, S. Adler, S. Agarwal, L. Ahmad, I. Akkaya, F. L. Aleman, D. Almeida, J. Al-tenschmidt, S. Altman, S. Anadkat, et al. Gpt-4 technical report. *arXiv preprint arXiv:2303.08774*, 2023.
- Y. Balaji, S. Nah, X. Huang, A. Vahdat, J. Song, Q. Zhang, K. Kreis, M. Aittala, T. Aila, S. Laine, et al. ediff-i: Text-to-image diffusion models with an ensemble of expert denoisers. *arXiv preprint arXiv:2211.01324*, 2022.
- J. Barros and R. I. Diego. On the use of the hanning window for harmonic analysis in the standard framework. *IEEE transactions on power delivery*, 21(1):538–539, 2005.
- A. Blattmann, T. Dockhorn, S. Kulal, D. Mendeleevitch, M. Kilian, D. Lorenz, Y. Levi, Z. English, V. Voleti, and A. Letts. Stable video diffusion: Scaling latent video diffusion models to large datasets. *arXiv preprint arXiv:2311.15127*, 2023a.
- A. Blattmann, R. Rombach, H. Ling, T. Dockhorn, S. W. Kim, S. Fidler, and K. Kreis. Align your latents: High-resolution video synthesis with latent diffusion models. In *Proceedings of the IEEE/CVF Conference on Computer Vision and Pattern Recognition*, pages 22563–22575, 2023b.
- M. Cao, X. Wang, Z. Qi, Y. Shan, X. Qie, and Y. Zheng. Masactrl: Tuning-free mutual self-attention control for consistent image synthesis and editing. In *Proceedings of the IEEE/CVF International Conference on Computer Vision*, pages 22560–22570, 2023.
- M. Caron, H. Touvron, I. Misra, H. Jégou, J. Mairal, P. Bojanowski, and A. Joulin. Emerging properties in self-supervised vision transformers. In *Proceedings of the IEEE/CVF international conference on computer vision*, pages 9650–9660, 2021.
- H. Chen, M. Xia, Y. He, Y. Zhang, X. Cun, S. Yang, J. Xing, Y. Liu, Q. Chen, X. Wang, et al. Videocrafter1: Open diffusion models for high-quality video generation. *arXiv preprint arXiv:2310.19512*, 2023.
- H. Chen, Y. Zhang, X. Cun, M. Xia, X. Wang, C. Weng, and Y. Shan. Videocrafter2: Overcoming data limitations for high-quality video diffusion models. In *Proceedings of the IEEE/CVF Conference on Computer Vision and Pattern Recognition*, pages 7310–7320, 2024.

- Q. Dong, L. Li, D. Dai, C. Zheng, J. Ma, R. Li, H. Xia, J. Xu, Z. Wu, and T. Liu. A survey on in-context learning. *arXiv preprint arXiv:2301.00234*, 2022.
- Y. Dong, J. Cordonnier, and A. Loukas. Attention is not all you need: Pure attention loses rank doubly exponentially with depth. In *International Conference on Machine Learning*, pages 2793–2803. PMLR, 2021.
- L. Durak and O. Arikan. Short-time fourier transform: two fundamental properties and an optimal implementation. *IEEE Transactions on Signal Processing*, 51(5):1231–1242, 2003.
- GenmoAI. GenmoAI Models: Open-Source Video Generation Models. <https://github.com/genmoai/models>, 2024.
- D. Griffin and J. Lim. Signal estimation from modified short-time fourier transform. *IEEE Transactions on acoustics, speech, and signal processing*, 32(2):236–243, 1984.
- Y. Guo, C. Yang, A. Rao, Z. Liang, Y. Wang, Y. Qiao, M. Agrawala, D. Lin, and B. Dai. Animatediff: Animate your personalized text-to-image diffusion models without specific tuning. *arXiv preprint arXiv:2307.04725*, 2023.
- W. Harvey, S. Naderiparizi, V. Masrani, C. Weillbach, and F. Wood. Flexible diffusion modeling of long videos. *Advances in Neural Information Processing Systems*, 35:27953–27965, 2022.
- R. Henschel, L. Khachatryan, D. Hayrapetyan, H. Poghosyan, V. Tadevosyan, Z. Wang, S. Navasardyan, and H. Shi. Streamingt2v: Consistent, dynamic, and extendable long video generation from text. *arXiv preprint arXiv:2403.14773*, 2024.
- J. Ho, T. Salimans, A. Gritsenko, W. Chan, M. Norouzi, and D. J. Fleet. Video diffusion models. *Advances in Neural Information Processing Systems*, 35:8633–8646, 2022.
- L. Hu. Animate anyone: Consistent and controllable image-to-video synthesis for character animation. In *Proceedings of the IEEE/CVF Conference on Computer Vision and Pattern Recognition*, pages 8153–8163, 2024.
- Z. Huang, Y. He, J. Yu, F. Zhang, C. Si, Y. Jiang, Y. Zhang, T. Wu, Q. Jin, N. Chanpaisit, et al. Vbench: Comprehensive benchmark suite for video generative models. In *Proceedings of the IEEE/CVF Conference on Computer Vision and Pattern Recognition*, pages 21807–21818, 2024.
- A. Janssen. Optimality property of the gaussian window spectrogram. *IEEE transactions on signal processing*, 39(1):202–204, 1991.
- J. Kim, J. Kang, J. Choi, and B. Han. FIFO-Diffusion: Generating infinite videos from text without training. *arXiv preprint arXiv:2405.11473*, 2024a.
- Y. Kim, G. Hwang, and E. Park. Diffusehigh: Training-free progressive high-resolution image synthesis through structure guidance. *arXiv preprint arXiv:2406.18459*, 2024b.
- Z. Li, Z. Zhu, L. Han, Q. Hou, C. Guo, and M. Cheng. Amt: All-pairs multi-field transforms for efficient frame interpolation. In *Proceedings of the IEEE/CVF Conference on Computer Vision and Pattern Recognition*, pages 9801–9810, 2023.

- Z. Li, R. Tucker, N. Snavely, and A. Holynski. Generative image dynamics. In *Proceedings of the IEEE/CVF Conference on Computer Vision and Pattern Recognition*, pages 24142–24153, 2024.
- J. H. Liew, H. Yan, D. Zhou, and J. Feng. Magicmix: Semantic mixing with diffusion models. *arXiv preprint arXiv:2210.16056*, 2022.
- Y. Liu, X. Cun, X. Liu, X. Wang, Y. Zhang, H. Chen, Y. Liu, T. Zeng, R. Chan, and Y. Shan. Evalcrafter: Benchmarking and evaluating large video generation models. In *Proceedings of the IEEE/CVF Conference on Computer Vision and Pattern Recognition*, pages 22139–22149, 2024.
- Y. Lu, Y. Liang, L. Zhu, and Y. Yang. Freelong: Training-free long video generation with spectralblend temporal attention. *arXiv preprint arXiv:2407.19918*, 2024.
- G. Oh, J. Jeong, S. Kim, W. Byeon, J. Kim, S. Kim, H. Kwon, and S. Kim. Mtv: Multi-text video generation with text-to-video models. *arXiv preprint arXiv:2312.04086*, 2023.
- OpenAI. Video Generation Models as World Simulators. <https://openai.com/index/video-generation-models-as-world-simulators/>, 2024.
- PKU-Yuan Lab and Tuzhan AI etc. Open-sora-plan, April 2024. URL <https://doi.org/10.5281/zenodo.10948109>.
- H. Qiu, M. Xia, Y. Zhang, Y. He, X. Wang, Y. Shan, and Z. Liu. Freenoise: Tuning-free longer video diffusion via noise rescheduling. *arXiv preprint arXiv:2310.15169*, 2023.
- A. Radford, J. W. Kim, C. Hallacy, A. Ramesh, G. Goh, S. Agarwal, G. Sastry, A. Askell, P. Mishkin, J. Clark, et al. Learning transferable visual models from natural language supervision. In *International conference on machine learning*, pages 8748–8763. PMLR, 2021.
- A. Ramesh, P. Dhariwal, A. Nichol, C. Chu, and M. Chen. Hierarchical text-conditional image generation with clip latents. *arXiv preprint arXiv:2204.06125*, 1(2):3, 2022.
- D. Ruhe, J. Heek, T. Salimans, and E. Hoogeboom. Rolling diffusion models. *arXiv preprint arXiv:2402.09470*, 2024.
- U. Singer, A. Polyak, T. Hayes, X. Yin, J. An, S. Zhang, Q. Hu, H. Yang, O. Ashual, O. Gafni, et al. Make-a-video: Text-to-video generation without text-video data. In *The Eleventh International Conference on Learning Representations*, 2022.
- Zachary Teed and Jia Deng. Raft: Recurrent all-pairs field transforms for optical flow. In *16th European Conference on Computer Vision (ECCV 2020)*, pages 402–419. Springer, 2020.
- F. Wang, W. Chen, G. Song, H. Ye, Y. Liu, and H. Li. Gen-l-video: Multi-text to long video generation via temporal co-denoising. *arXiv preprint arXiv:2305.18264*, 2023a.
- J. Wang, H. Yuan, D. Chen, Y. Zhang, X. Wang, and S. Zhang. Modelscape text-to-video technical report. *arXiv preprint arXiv:2308.06571*, 2023b.

- Y. Wang, X. Chen, X. Ma, S. Zhou, Z. Huang, Y. Wang, C. Yang, Y. He, J. Yu, P. Yang, et al. Lavie: High-quality video generation with cascaded latent diffusion models. *arXiv preprint arXiv:2309.15103*, 2023c.
- W. Weng, R. Feng, Y. Wang, Q. Dai, C. Wang, D. Yin, Z. Zhao, K. Qiu, J. Bao, Y. Yuan, et al. Art-v: Auto-regressive text-to-video generation with diffusion models. In *Proceedings of the IEEE/CVF Conference on Computer Vision and Pattern Recognition*, pages 7395–7405, 2024.
- T. Wu, C. Si, Y. Jiang, Z. Huang, and Z. Liu. Freeinit: Bridging initialization gap in video diffusion models. In *European Conference on Computer Vision*, pages 378–394. Springer, 2025.
- Z. Yang, J. Teng, W. Zheng, M. Ding, S. Huang, J. Xu, Y. Yang, W. Hong, X. Zhang, G. Feng, et al. Cogvideox: Text-to-video diffusion models with an expert transformer. *arXiv preprint arXiv:2408.06072*, 2024.
- S. Yin, C. Wu, H. Yang, J. Wang, X. Wang, M. Ni, Z. Yang, L. Li, S.g Liu, and F. Yang. Nuwa-xl: Diffusion over diffusion for extremely long video generation. *arXiv preprint arXiv:2303.12346*, 2023.
- Z. Zheng, X. Peng, T. Yang, C. Shen, S. Li, H. Liu, Y. Zhou, T. Li, and Y. You. Open-sora: Democratizing efficient video production for all, March 2024. URL <https://github.com/hpcaitech/Open-Sora>.
- D. Zhou, W. Wang, H. Yan, W. Lv, Y. Zhu, and J. Feng. Magicvideo: Efficient video generation with latent diffusion models. *arXiv preprint arXiv:2211.11018*, 2022.
- Y. Zhou, D. Zhou, M. Cheng, J. Feng, and Q. Hou. Storydiffusion: Consistent self-attention for long-range image and video generation. *arXiv preprint arXiv:2405.01434*, 2024.

Appendix

A Pseudocode of Prompt Interpolation

We present the pseudocode of our prompt interpolation pipeline in Algorithm 2. In our experiment, we prescribe the order of components $\mathcal{C} = [c_1, c_2, c_3, c_4, c_5]$ to be [*The subject, The Action, The Place, The Time, Video Quality Description*], and ChatGPT is adopted to complete this organization (see Fig. 8).

Algorithm 2 PROMPTBLEND

```
1: Input: Prompts  $\{P_i\}_{i=1}^m$ , starting and ending points of each prompt  $\{(n_i^s, n_i^e)\}_{i=1}^m$ , the
   prescribed order of components  $\mathcal{C} = [c_1, c_2, c_3, c_4, c_5]$ , tokenizer  $\mathcal{T}$  and token embedder  $\mathcal{E}$ ,
   frame number  $n$ , denoising time step interval  $[t_1, t_2]$  and U-Net layer index  $D$ .
2: // Prompt Embedding Alignment
3: Call LLM to organize the prompts  $\{P_i\}_{i=1}^m$  into the format:  $[P_{i,1}, P_{i,2}, P_{i,3}, P_{i,4}, P_{i,5}]$  according
   to the prescribed order  $\mathcal{C}$ .
4: for  $k = 1, \dots, 5$  do
5:    $M = \max_i \left\{ \text{length}(\mathcal{T}(P_{i,k})) \right\}_{i=1}^m$ 
6:   for  $i = 1, \dots, m$  do
7:     Repeat  $\mathcal{T}(P_{i,k})$  until its length reaches  $M$  to obtain  $\overline{\mathcal{T}(P_{i,k})}$ 
8:   end for
9: end for
10: for  $i = 1, \dots, m$  do
11:    $\overline{\mathcal{T}(P_i)} \leftarrow \text{concat}(\{\overline{\mathcal{T}(P_{i,k})}\}_{k=1}^5)$ 
12:   Embed the aligned tokens  $\overline{\mathcal{P}}_i \leftarrow \mathcal{E}(\overline{\mathcal{T}(P_i)})$ 
13: end for
14: // Application of Interpolation to Networks
15:  $i \leftarrow 1$ 
16: for  $n = 1, \dots, n_m^e$  do
17:   if  $n \in [n_i^e, n_{i+1}^s)$  then
18:      $a_n \leftarrow (n - n_i^e) / (n_{i+1}^s - n_i^e)$ 
19:     if  $t \in [t_1, t_2]$  or  $d \geq D$  then
20:        $\mathcal{P}_C \leftarrow (1 - a_n)\overline{\mathcal{P}}_i + a_n\overline{\mathcal{P}}_{i+1}$ 
21:     else
22:        $\mathcal{P}_C \leftarrow \overline{\mathcal{P}}_i$ 
23:     end if
24:   else if  $n = n_{i+1}^s$  then
25:      $\mathcal{P}_C \leftarrow \overline{\mathcal{P}}_{i+1}$ ,  $i \leftarrow i + 1$ 
26:   end if
27: end for
```

B Related Works

Video Diffusion Models Video diffusion models are an emerging class of generative models that extend the success of diffusion models from static images to video generation. While image diffusion models, such as DALL-E 2 Ramesh et al. [2022] and Stable Diffusion Blattmann et al. [2023b], have demonstrated remarkable capabilities in generating high-quality images from text prompts, applying these methods to videos introduces additional complexity due to the need for both spatial and temporal coherence. Video generation requires not only high-quality, realistic frames but also consistent motion and appearance across frames, posing unique challenges that are not present in image generation tasks.

Several notable advancements have been made in this field. Video Diffusion Models (VDM) Ho et al. [2022] first adapted diffusion techniques to video by incorporating temporal information through 3D convolutions and cross-frame attention, providing a foundational approach for video generation. Following VDM, a list of video diffusion models has been proposed, such as Make-A-Video Singer et al. [2022], MagicVideo Zhou et al. [2022], and so on. VideoCrafter1 Chen et al. [2023] proposes the first open-source I2V foundation model capable of transforming a given image into a video clip while maintaining content preservation constraints and VideoCrafter2 Chen et al. [2024] updates the former version to a high-quality video generation model. Open-Sora [Zheng et al., 2024] and Open-Sora-Plan [PKU-Yuan Lab and Tuzhan AI etc., 2024] are open-source text-to-video generation models that aim at replicating and advancing OpenAI’s text-to-video generation model, Sora OpenAI [2024]. Recent advances in video synthesis have introduced powerful models such as Mochi GenmoAI [2024] and CogVideoX Yang et al. [2024], each of which addresses key challenges in generating realistic and coherent videos. With improved fine-grained text control, higher resolution, and enhanced temporal coherence, CogVideoX can produce realistic video sequences that align closely with input prompts. Mochi is an open state-of-the-art video generation model with high-fidelity motion and strong prompt adherence.

Long Video Generation with Diffusion Models Although the tremendous successes achieved by the video diffusion models, the window sizes of pretrained models are only 16-24 [Chen et al., 2024, Guo et al., 2023, Wang et al., 2023b]. A direct way to generate long videos is to extend the window sizes of pretrained models, i.e., they are trained to denoise more frames concurrently. Open-Sora [Zheng et al., 2024] and Open-Sora-Plan [PKU-Yuan Lab and Tuzhan AI etc., 2024] are two representative works in this direction, and they can denoise up to 93 frames concurrently. Another line of work attempts to train the auto-regressive video diffusion models. In these models, the generation of the next chunk of frames is based on the already generated frame. StreamingT2V [Henschel et al., 2024], ART-V Weng et al. [2024], and MTVG [Oh et al., 2023] all train models to take history frames as inputs and generate the next chunk of frames based on the history. A flexible history sampling method for training is introduced in Harvey et al. [2022]. Some works also try to generate long videos by first generating key frames and then interpolating these frames. NUWA-XL [Yin et al., 2023] trains models to predict the middle frame of two frames. Applying this many times, this method can generate a long video. StoryDiffusion [Zhou et al., 2024] first generates several key consistent frames and uses these frames for smooth interpolation. All the mentioned works trained new diffusion models to generate long videos, and a line of works aims to generate long videos in a training-free manner. FreeNoise [Qiu et al., 2023] and FreeLong [Lu et al.,

2024] extend the window size of diffusion models by taking a lot of frames as inputs of a single diffusion model and restricting the attention window size for each frame along the temporal axis. Gen-L-Video [Wang et al., 2023a] extends the window sizing by parallelly using multiple video diffusion models with overlaps. The predicted noises for the overlapped clips are weighted versions of predictions from multiple models. FIFO-Diffusion [Kim et al., 2024a] generates long videos in an auto-regressive way. In contrast to the previous methods, FIFO-Diffusion denoises frames at different noise levels organized as a queue. At each denoising step, a clean frame is popped from the queue, and a Gaussian noise is pushed into the queue.

Frequency Analysis in Video Diffusion Models The frequency analysis methods are widely used in the computer vision community. The existing works about video diffusion models also adopt frequency analysis for quality improvement. Freeinit [Wu et al., 2025] adopts Fourier Transform (FT) to maintain the low-frequency information and continuously refine the high-frequency information. Freelong [Lu et al., 2024] adopts FT to enhance the local information while preserving the global information. Kim et al. [Kim et al., 2024b] have shown that the Wavelet transform is effective in distinguishing information at different granularities in the super-resolution algorithm. The frequency analysis also demonstrates its efficacy in generating videos of periodic motions [Li et al., 2024]. We note that these works adopt frequency analysis methods just out of vague intuitions. In contrast, our work is the first work that builds a religious theoretical analysis of the time-frequency methods, which provides firm support for the intuitions of time-frequency methods in video diffusion models.

C Limitation

Our current method is specifically designed for video diffusion models using 2D + 1D temporal attention and is not directly applicable to architectures with 3D temporal attention. Extending our approach to support 3D temporal attention is an avenue for future work.

D Notation

Let $[N] := \{0, \dots, N - 1\}$. For a real number $x \in \mathbb{R}$, the largest integer that is not larger than x is denoted as $\lfloor x \rfloor$. For two sequences $\{(x_i, y_i)\}_{i \in [N]}$, their discrete convolution is defined as $(x * y)_i = \sum_{j=0}^{N-1} x_j y_{i-j}$. We respectively use $I_{N \times N} \in \mathbb{R}^{N \times N}$ and $I_N \in \mathbb{R}^N$ to denote the identity matrix of size $N \times N$ and all-ones vector of size N . For a matrix $A \in \mathbb{R}^{m \times n}$, we use $A_{i,j}$, $A_{i,:}$, and $A_{:,j}$ to denote the (i, j) component, the i -th row, and the j -th column of A , respectively.

E Proof of Theorem 4.4

The proof of Theorem 4.4 consists of the following three steps.

- Decompose the DSTFT of signals x and y .
- Bound each term in the decompositions.
- Conclude the proof.

Step 1: Decompose the DSTFT of signals x and y .

In the whole proof, we assume that

$$A_{0,0}^X = \min_{i \in [N]} A_{i,i}^X$$

without loss of generality. Otherwise, we can replace the index 0 in the proof with $i^* = \operatorname{argmin}_{i \in [N]} A_{i,i}^X$. We would like to express the results of the attention module as follows:

$$x_i = \sum_{j=0}^{N-1} A_{i,j}^X v_j = \sum_{j=0}^{N-1} A_{i,i+m}^X v_{i+m} = \sum_{j=0}^{N-1} A_{0,m}^X v_{i+m} + \sum_{j=0}^{N-1} (A_{i,i+m}^X - A_{0,m}^X) v_{i+m}.$$

We define the flipped version \bar{A}^X of A^X as $\bar{A}_{i,j}^X = A_{i,-j}^X$. Then we have that

$$x_i = (\bar{A}_{0,:}^X * v)_i + \sum_{j=0}^{N-1} (A_{i,i+m}^X - A_{0,m}^X) v_{i+m} = (\bar{A}_{0,:}^X * v)_i + \Delta_i^X, \quad (\text{E.1})$$

where $*$ denotes the convolution between two signals, and Δ_i^X is the difference term. Similarly, we have that

$$y_i = (\bar{A}_{0,:}^Y * v)_i + \sum_{j=0}^{N-1} (A_{i,i+m}^Y - A_{0,m}^Y) v_{i+m} = (\bar{A}_{0,:}^Y * v)_i + \Delta_i^Y, \quad (\text{E.2})$$

$$x_i^{\text{dyn}} = (\bar{A}_{0,:}^{X,D} * v)_i + \sum_{j=0}^{N-1} (A_{i,i+m}^{X,D} - A_{0,m}^{X,D}) v_{i+m} = (\bar{A}_{0,:}^{X,D} * v)_i + \Delta_i^{X,D}, \quad (\text{E.3})$$

where \bar{A}^Y and $\bar{A}^{X,D}$ are the flipped versions of A^Y and $A^{X,D}$, respectively. Then we would like to deduce the relationship between $A_{0,:}^X$ and $A_{0,:}^Y$. According to the definition of A^X and A^Y , we have that

$$\begin{aligned} A_{0,i}^Y &= \frac{\exp(q_0^\top k_i)}{\exp(q_0^\top k_0 - \alpha) + \sum_{j=1}^{N-1} \exp(q_0^\top k_j)} \\ &= \frac{A_{0,i}^X}{\exp(-\alpha) \cdot A_{0,0}^X + \sum_{j=1}^{N-1} A_{0,j}^X} \\ &= \frac{A_{0,i}^X}{1 - (1 - \exp(-\alpha)) \cdot A_{0,0}^X} \end{aligned}$$

for $i \neq 0$, where the last equality follows from the fact that the sum over all $A_{0,i}^X$ is equal to 1. For $i = 0$, we similarly have that

$$A_{0,0}^Y = \frac{\exp(-\alpha) \cdot A_{0,0}^X}{1 - (1 - \exp(-\alpha)) \cdot A_{0,0}^X}.$$

Combining these two equations, we have that

$$A_{0,i}^Y - A_{0,i}^X = \begin{cases} \frac{(\exp(-\alpha) - 1)(1 - A_{0,0}^X)}{1 - (1 - \exp(-\alpha))A_{0,0}^X} \cdot A_{0,0}^X & \text{if } i = 0, \\ \frac{(1 - \exp(-\alpha))A_{0,0}^X}{1 - (1 - \exp(-\alpha))A_{0,i}^X} \cdot A_{0,i}^X & \text{if } i \neq 0. \end{cases}$$

Here the equality follows from some simple algebraic manipulations. Then we decompose $A_{0,:}^Y$ as

$$\begin{aligned}
A_{0,:}^Y &= \left(1 - \frac{(1 - \exp(-\alpha))(1 - A_{0,0}^X)}{1 - (1 - \exp(-\alpha))A_{0,0}^X} \right) \cdot A_{0,:}^X + \Delta^A \\
&= \frac{\exp(-\alpha)}{1 - (1 - \exp(-\alpha))A_{0,0}^X} \cdot A_{0,:}^X + \Delta^A \\
&= \iota(\alpha, A_{0,0}^X) \cdot A_{0,:}^X + \Delta^A,
\end{aligned} \tag{E.4}$$

where Δ^A is defined as

$$\Delta^A = \frac{1 - \exp(-\alpha)}{1 - (1 - \exp(-\alpha))A_{0,0}^X} \cdot A_{0,:}^{X,D} = \lambda(\alpha, A_{0,0}^X) \cdot A_{0,:}^{X,D}.$$

Here $A^{X,D}$ represents the low-frequency part of A^X , which is defined in Section 4. From the definition of DSTFT, we have that

$$\text{DSTFT}(y, \psi, \tau, k) = \text{DFT}(y \cdot \psi_{\cdot-\tau}, k) = [\text{DFT}(y, \cdot) * \text{DFT}(\psi_{\cdot-\tau}, \cdot)]_k \tag{E.5}$$

for any frequency $k \in [N]$ and shift $\tau \in [N]$, where $\psi_{\cdot-\tau}$ is the signal ψ that is shifted to right by τ units. The last equality follows from the fact that DFT of the product of two signals is equal to the convolution of the DFTs of these two signals. For the first term in the right-hand side of Eqn. (E.5), combining Eqns. (E.2) and (E.4), we obtain

$$\begin{aligned}
&\text{DFT}(y, k) \\
&= \text{DFT}(\bar{A}_{0,:}^Y * v, k) + \text{DFT}(\Delta^Y, k) \\
&= \text{DFT}(\bar{A}_{0,:}^Y, k) \cdot \text{DFT}(v, k) + \text{DFT}(\Delta^Y, k) \\
&= [\iota(\alpha, A_{0,0}^X) \cdot \text{DFT}(\bar{A}_{0,:}^X, k) + \text{DFT}(\bar{\Delta}^A, k)] \text{DFT}(v, k) \\
&\quad + \text{DFT}(\Delta^Y, k),
\end{aligned} \tag{E.6}$$

where the second equality also follows from the fact that DFT of the convolution of two signals is equal to the multiplication of the DFTs of these two signals, and $\bar{\Delta}^A$ is the flipped version of Δ^A . Combining Eqns. (E.5) and (E.6), we obtain

$$\begin{aligned}
&\text{DSTFT}(y, \psi, \tau, k) \\
&= \iota(\alpha, A_{0,0}^X) \left[(\text{DFT}(\bar{A}_{0,:}^X, \cdot) \text{DFT}(v, \cdot)) * \text{DFT}(\psi_{\cdot-\tau}, \cdot) \right]_k \\
&\quad + \lambda(\alpha, A_{0,0}^X) \left[(\text{DFT}(\bar{A}_{0,:}^{X,D}, \cdot) \text{DFT}(v, \cdot)) * \text{DFT}(\psi_{\cdot-\tau}, \cdot) \right]_k \\
&\quad + [\text{DFT}(\Delta^Y, \cdot) * \text{DFT}(\psi_{\cdot-\tau}, \cdot)]_k \\
&= \iota(\alpha, A_{0,0}^X) \cdot \text{DSTFT}(\bar{A}_{0,:}^X * v, \psi, \tau, k) \\
&\quad + \lambda(\alpha, A_{0,0}^X) \cdot \text{DSTFT}(\bar{A}_{0,:}^{X,D} * v, \psi, \tau, k) \\
&\quad + [\text{DFT}(\Delta^Y, \cdot) * \text{DFT}(\psi_{\cdot-\tau}, \cdot)]_k,
\end{aligned} \tag{E.7}$$

where the first equality follows from the linearity of DFT. Similarly, we can decompose the DSTFT of x and x^D as

$$\text{DSTFT}(x, \psi, \tau, k) = \text{DSTFT}(\bar{A}_{0,:}^X * v, \psi, \tau, k) + [\text{DFT}(\Delta^X, \cdot) * \text{DFT}(\psi_{\cdot-\tau}, \cdot)]_k \tag{E.8}$$

$$\text{DSTFT}(x^D, \psi, \tau, k) = \text{DSTFT}(\bar{A}_{0,:}^{X,D} * v, \psi, \tau, k) + [\text{DFT}(\Delta^{X,D}, \cdot) * \text{DFT}(\psi_{\cdot-\tau}, \cdot)]_k \tag{E.9}$$

Step 2: Bound each term in the decompositions.

We would like to bound each term in the decompositions in Eqn. (E.7) and (E.8). We first bound the norms of $\text{DFT}(\Delta^X, k)$ and $\text{DFT}(\Delta^Y, k)$. For $\text{DFT}(\Delta^X, k)$, we have that

$$\begin{aligned}
& |\text{DFT}(\Delta^X, k)| \\
&= \left| \sum_{n=0}^{N-1} \sum_{j=0}^{N-1} (A_{n,n+m}^X - A_{0,m}^X) v_{n+m} \exp\left(-i \frac{2\pi kn}{N}\right) \right| \\
&\leq \sum_{n=0}^{N-1} \sum_{j=0}^{N-1} |A_{n,n+m}^X - A_{0,m}^X| \cdot B_V \\
&= O\left(\frac{B_V}{N^{\gamma-2}}\right), \tag{E.10}
\end{aligned}$$

where the last inequality results from Assumption 4.2. Similarly, we have that

$$|\text{DFT}(\Delta^{X,D}, k)| = O\left(\frac{B_V}{N^{\gamma-2}}\right), \tag{E.11}$$

For $\text{DFT}(\Delta^Y, k)$, we first bound the difference between $A_{n,n+m}^Y$ and $A_{0,m}^Y$. From the definition of A^Y , for $m \neq 0$, we have that

$$\begin{aligned}
& A_{n,n+m}^Y - A_{0,m}^Y \\
&= \frac{A_{n,n+m}^X}{\exp(-\alpha) \cdot A_{n,n}^X + \sum_{l \neq 0} A_{n,n+l}^X} - \frac{A_{0,m}^X}{\exp(-\alpha) \cdot A_{0,0}^X + \sum_{l \neq 0} A_{0,l}^X} \\
&= \left(\exp(-\alpha) \cdot A_{n,n}^X + \sum_{l \neq 0} A_{n,n+l}^X \right)^{-1} \cdot \left(\exp(-\alpha) \cdot A_{0,0}^X + \sum_{l \neq 0} A_{0,l}^X \right)^{-1} \cdot \Delta,
\end{aligned}$$

where the second inequality follows from some simple algebraic manipulations, and the term Δ is defined as

$$\begin{aligned}
\Delta &= \exp(-\alpha) \cdot [(A_{0,0}^X - A_{n,n}^X)A_{n,n+m}^X + (A_{n,n+m}^X - A_{0,m}^X)A_{n,n}^X \\
&\quad + \sum_{l \neq 0} A_{n,n+m}^X (A_{0,l}^X - A_{n,n+l}^X) + \sum_{l \neq 0} A_{n,n+l}^X (A_{n,n+m}^X - A_{0,m}^X)].
\end{aligned}$$

Using the triangle inequality, we obtain

$$|A_{n,n+m}^Y - A_{0,m}^Y| \leq O\left(\frac{\exp(2\alpha)}{N^{\gamma-1}}\right) \text{ for } m \neq 0. \tag{E.12}$$

For case $m = 0$, we similarly have that $|A_{n,n}^Y - A_{0,0}^Y| = O(\exp(2\alpha)N^{-\gamma+1})$. Following the same computation of Eqns. (E.10) and (E.12), we have that

$$|\text{DFT}(\Delta^Y, k)| = O\left(\frac{B_V}{N^{\gamma-3}}\right). \tag{E.13}$$

Step 3: Conclude the proof.

We conclude the proof in this final step. For the inconsistency error of the new signal y , we obtain

$$\begin{aligned}
& \sum_{k=k_{\text{thre}}}^{\lfloor N/2 \rfloor} |\text{DSTFT}(y, \psi, \tau, k)| \\
& \leq \iota(\alpha, A_{0,0}^X) \cdot \left[\sum_{k=k_{\text{thre}}}^{\lfloor N/2 \rfloor} |\text{DSTFT}(x, \psi, \tau, k)| + \left| [\text{DFT}(\Delta^X, \cdot) * \text{DFT}(\psi_{\cdot-\tau}, \cdot)]_k \right| \right] \\
& \quad + \lambda(\alpha, A_{0,0}^X) \cdot \left[\sum_{k=k_{\text{thre}}}^{\lfloor N/2 \rfloor} |\text{DSTFT}(x^D, \psi, \tau, k)| + \left| [\text{DFT}(\Delta^{X,D}, \cdot) * \text{DFT}(\psi_{\cdot-\tau}, \cdot)]_k \right| \right] \\
& \quad + \sum_{k=k_{\text{thre}}}^{\lfloor N/2 \rfloor} \left| [\text{DFT}(\Delta^Y, \cdot) * \text{DFT}(\psi_{\cdot-\tau}, \cdot)]_k \right| \\
& \leq (\iota(\alpha, A_{0,0}^X) + \kappa \lambda(\alpha, A_{0,0}^X)) \cdot \sum_{k=k_{\text{thre}}}^{\lfloor N/2 \rfloor} |\text{DSTFT}(x, \psi, \tau, k)| + O\left(\frac{B_V}{N^{\gamma-4}}\right), \tag{E.14}
\end{aligned}$$

where the first inequality follows from Eqns. (E.7), (E.8), (E.9) and the triangle inequality, and the second inequality follows from Assumption 4.3 and Eqns. (E.10), (E.11), and (E.13). Since $\kappa < 1 - A_{0,0}^X$, we note that

$$\alpha := \log \frac{1 - \kappa - A_{0,0}^X \cdot \eta}{\eta(1 - A_{0,0}^X) - \kappa}$$

satisfies that $\iota(\alpha, A_{0,0}^X) + \kappa \cdot \lambda(\alpha, A_{0,0}^X) = \eta$. Since $\liminf_{N \rightarrow \infty} \mathbb{E}(x^{(N)}, \tau) \geq C$, we conclude that the constructed α guarantees that

$$\begin{aligned}
& \sum_{k=k_{\text{thre}}}^{\lfloor N/2 \rfloor} |\text{DSTFT}(y, \psi, \tau, k)| \\
& \leq \eta \sum_{k=k_{\text{thre}}}^{\lfloor N/2 \rfloor} |\text{DSTFT}(x, \psi, \tau, k)| + o\left(\sum_{k=k_{\text{thre}}}^{\lfloor N/2 \rfloor} |\text{DSTFT}(x, \psi, \tau, k)|\right).
\end{aligned}$$

This concludes the proof of Theorem 4.4.

F Additional Implementation Details

F.1 User Study Setup

In our user study, participants were presented with pairs of videos generated using the long video generation pipeline, either with or without our proposed method/methods. Participants were asked to select the video that (1) matched the prompt and (2) exhibited greater consistency in subject and background, and smoothness in motion. A total of 704 samples were collected, with over 140 samples for each method. The percentages shown in Fig. 6 represent the proportion of positive selections for our method, calculated as the number of favorable choices for our method divided by the total samples for that method.

F.2 Metrics

- Subject Consistency (SC): To assess the consistency of the subject in the video across all frames using DINO [Caron et al., 2021] feature similarity.
- Background Consistency (BC): To assess the consistency of the background across all frames using CLIP [Radford et al., 2021] feature similarity.
- Temporal Flickering (TF): To evaluate the consistency of the generated video at local and high-frequency details.
- Motion Smoothness (MS): To evaluate the quality of the movements and motions in the generated video by comparing the video interpolation result using Li et al. [2023].
- Warping Error (WE): To evaluate the temporal consistency using optical flow estimation network [Teed and Deng, 2020].
- CLIP-Temp Score (CTS): To assess the semantic consistency between each two frames by computing the cosine similarity of their CLIP [Radford et al., 2021] embeddings.

G Additional Ablation Study

Ablation study on the effect of prompt alignment on interpolation We compare the performance of prompt interpolation on original prompt inputs compared to those aligned with our proposed alignment method. To isolate the impact of prompt alignment, we conduct these experiments without TIA RA, and use the interpolated prompts directly as text conditioning for the transition frames. Since prompt alignment primarily enhances prompt interpolation, the analysis focuses on the transition frames. The results are illustrated in Fig. 7. In the examples without prompt alignment, breakdowns occur during the transitions as prompts are interpolated, likely due to the non-interpretability of these interpolated prompts. With prompt alignment, these issues are resolved, resulting in smoother and more consistent transitions.

H LLM Prompts for Input Prompts Organization

In our experiments, we utilize ChatGPT for prompt organization, with exact prompt are given in Fig. 8. The Required Components and their sequence in the ChatGPT prompts are customizable and can be adjusted to suit the user’s preferences, offering flexibility in adapting the prompts to different scenarios or tasks.

I Test Set

I.1 Single-Prompt Test Set

The single-prompt test set is given as follow:

1. A surfer is riding a wave in a tropical beach, high quality, 4K.
2. An old man is sitting on a bench in a quiet park, high quality, 4K.

3. A scenic hot air balloon is flying in sunrise, high quality, 4K.
4. A rainbow flag is flying in the wind in a sunny day, high quality, 4K.
5. A fountain is spraying water in the center of the garden, high quality, 4K.
6. A Ferris wheel is rotating in the amusement park during twilight, high quality, 4K.
7. A book is flipping its pages on a table, high quality, 4K.
8. A colony of penguins waddling on an Antarctic ice sheet, 4K, ultra HD.
9. A pair of tango dancers performing in Buenos Aires, 4K, high resolution.
10. A red balloon is flying higher and higher in the sunlit backyard, high quality, 4K.
11. A small boat is slowly sailing across the Seine River in the sunset, high quality, 4K.
12. A lotus is floating in a tranquil pond, high quality, 4K.
13. An athlete is running on the track in the noon sunlight, high quality, 4K.
14. A fat rabbit wearing a purple robe is walking through a fantasy landscape, high quality, 4K.
15. An astronaut is feeding ducks on a sunny afternoon, reflection from the water, high quality, 4K.
16. Santa Claus is dancing.
17. People dancing in room filled with fog and colorful lights.
18. A tiger eating raw meat on the street.
19. A graceful heron stood poised near the reflecting pools of the Duomo, adding a touch of tranquility to the vibrant surroundings.
20. A woman with a camera in hand joyfully skipped along the perimeter of the Duomo, capturing the essence of the moment.
21. Beside the ancient amphitheater of Taormina, a group of friends enjoyed a leisurely picnic, taking in the breath-taking views.
22. A camel resting on the snow field.
23. A gorilla eats a banana in Central Park.
24. Time-lapse of stormclouds during thunderstorm.
25. Around the lively streets of Corso Como, a fearless urban rabbit hopped playfully, seemingly unfazed by the fashionable surroundings.
26. A musk ox grazing on beautiful wildflowers.

27. A beagle reading a paper.
28. A beagle looking in the Louvre at a painting.
29. A squirrel watches with sweet eyes into the camera.
30. Men walking in the rain.
31. A squirrel in Antarctica, on a pile of hazelnuts cinematic.
32. A young girl making selfies with her phone in a crowded street.
33. Prague, Czech Republic. Heavy rain on the street.
34. A kitten resting on a ball of wool.

I.2 Multi-Prompt Test Set

We present the multi-prompt test set in Fig. 9.

J Additional Experiment Results

Qualitative results on single-prompt video generation The qualitative results of single-prompt video generation based on models FIFO, FreeNoise and StreamingT2V are displayed in Fig. 10, 11 and 12 respectively. These results highlight the effectiveness of our method in addressing inconsistencies commonly observed in generated videos, such as abrupt changes in object appearance or background transitions. By applying `T1ARA`, the generated videos exhibit enhanced temporal coherence, smoother motion, and improved overall quality, demonstrating its robustness across different models.

Qualitative results on multi-prompt video generation The qualitative results of multi-prompt video generation based on FIFO is presented in Fig. 13. By applying `T1ARA` and `PROMPTBLEND`, inconsistencies in the generated videos are greatly reduced, achieving smoother transitions between scenes and improved overall coherence.

K Possible Negative Societal Impacts

While our proposed methods `T1ARA` and `PROMPTBLEND` improve the consistency and quality of video generation using diffusion models, they also present potential risks of misuse. Enhanced video generation techniques could be exploited to create realistic but deceptive content, such as deepfakes or misleading media, with harmful societal consequences, including the spread of misinformation or manipulation of public opinion. Additionally, the ability to generate high-quality, seamless videos may pose privacy risks if applied to sensitive or unauthorized data. These concerns highlight the importance of ethical considerations and responsible usage of video generation technologies.

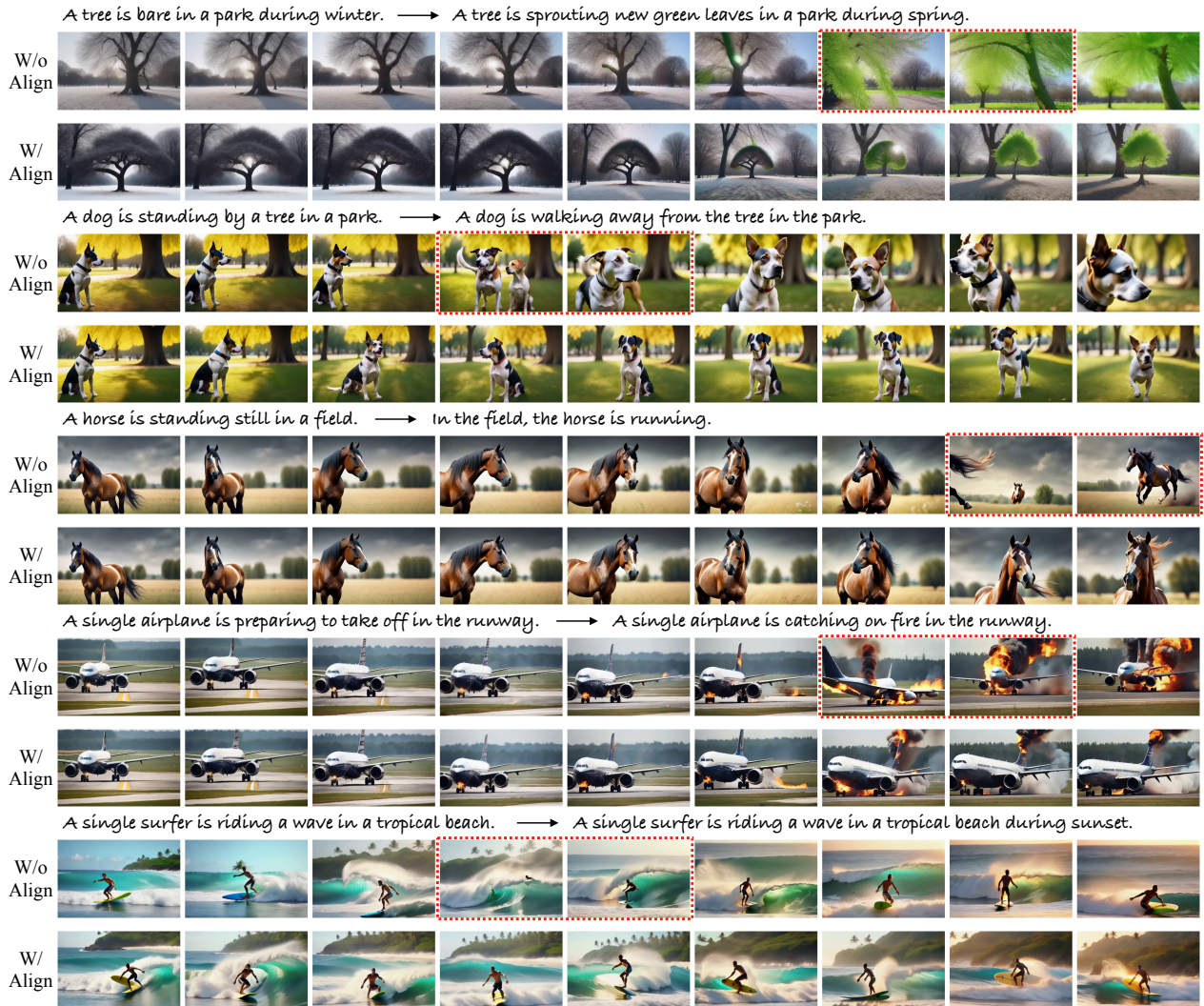


Figure 7: Ablation study on the effect of prompt alignment on interpolation. The experiment is conducted using FIFO. The first row of each example is the result with interpolation but without prompt alignment; the second row is the result with both interpolation and alignment. The displayed frames are sampled at fixed intervals. The poorly generated frames are marked with red dotted boxes.

ChatGPT Instruction

I would like you to play the role of **the prompt organizer** that reorganize { The Prompt } into a prompt of { The Required Components }.

You **extract** all { The Required Components } from the given prompt, **reorganize** them in { The Pre-defined Order }, and **add** “\$” between different components. While doing the organization, follow the given rules:

Rule 1: If there exists **extra descriptions** about The Action, count that part into The Action, e.g. the direction of The Action, the object of The Action.

Rule 2: The output is in **the exact form** of: A/The { **The Subject** }\$ { **The Action** }\$ { **The Place** }\$ { **The Time** }\$ { **Video Quality Description** }.

Rule 3: If one of the components **does not exist** (e.g. The Time), return a “ ” for that components, e.g. A/The { The Subject }\$ { The Action }\$ { The Place }\$\$ { Video Quality Description }.

Rule 4: Correct the **grammar** of the prompt with minimum modifications while keeping the “\$”s in their positions.

The Required Components : { **The Subject**, **The Action**, **The Place**, **The Time**, **Video Quality Description** }.

The Prompt : { user input }

Return only the sentence.

Figure 8: ChatGPT Instruction.

Multi-Prompt Test set

- Set 1: A tree is bare in a park during winter, high quality, 4K.
In the park during spring, new green leaves are sprouting on a tree, high quality, 4K.
- Set 2: A forest is quiet and still in the early morning, high quality, 4K.
In the morning light, animals awaken and bring life to the forest, high quality, 4K.
- Set 3: During the day, the mountain is visible under clear skies, high quality, 4K.
The mountain is shrouded in mist as the night falls, high quality, 4K.
- Set 4: At sunset, a scenic hot air balloon is flying, high quality, 4K.
A single scenic hot air balloon is flying in the night, high quality, 4K.
- Set 5: Under the bright sun, a mountain trail is clearly visible, high quality, 4K.
A mountain trail is shadowed and hard to see under thick clouds, high quality, 4K.
- Set 6: A park is empty and still at dawn, high quality, 4K.
During the morning, the park is lively with children playing, high quality, 4K.
- Set 7: A cat is sitting on a porch in the afternoon, high quality, 4K.
In the afternoon, a cat is lying down on the porch, high quality, 4K.
- Set 8: Next to a tree in the park, the dog stands still, high quality, 4K.
A dog is walking away from the tree in the park, high quality, 4K.
- Set 9: A horse is standing still in a field, high quality, 4K.
In the field, the horse is running, high quality, 4K.
- Set 10: On the runway, a single airplane prepares for takeoff, high quality, 4K.
A single airplane is catching on fire on the runway, high quality, 4K.
- Set 11: A single dark knight is riding on a black horse in the grassland, high quality, 4K.
In the grassland, a dark knight rides his black horse towards a misty forest, high quality, 4K.
- Set 12: A single surfer is riding a wave on a tropical beach, high quality, 4K.
During the sunset on a tropical beach, a single surfer is riding a wave, high quality, 4K.
- Set 13: In the dusk, the Seine River is gradually lighted up by streetlights, high quality, 4K.
The Seine River is occupied with boats in the dusk, high quality, 4K.

Figure 9: Multi-prompt test set.

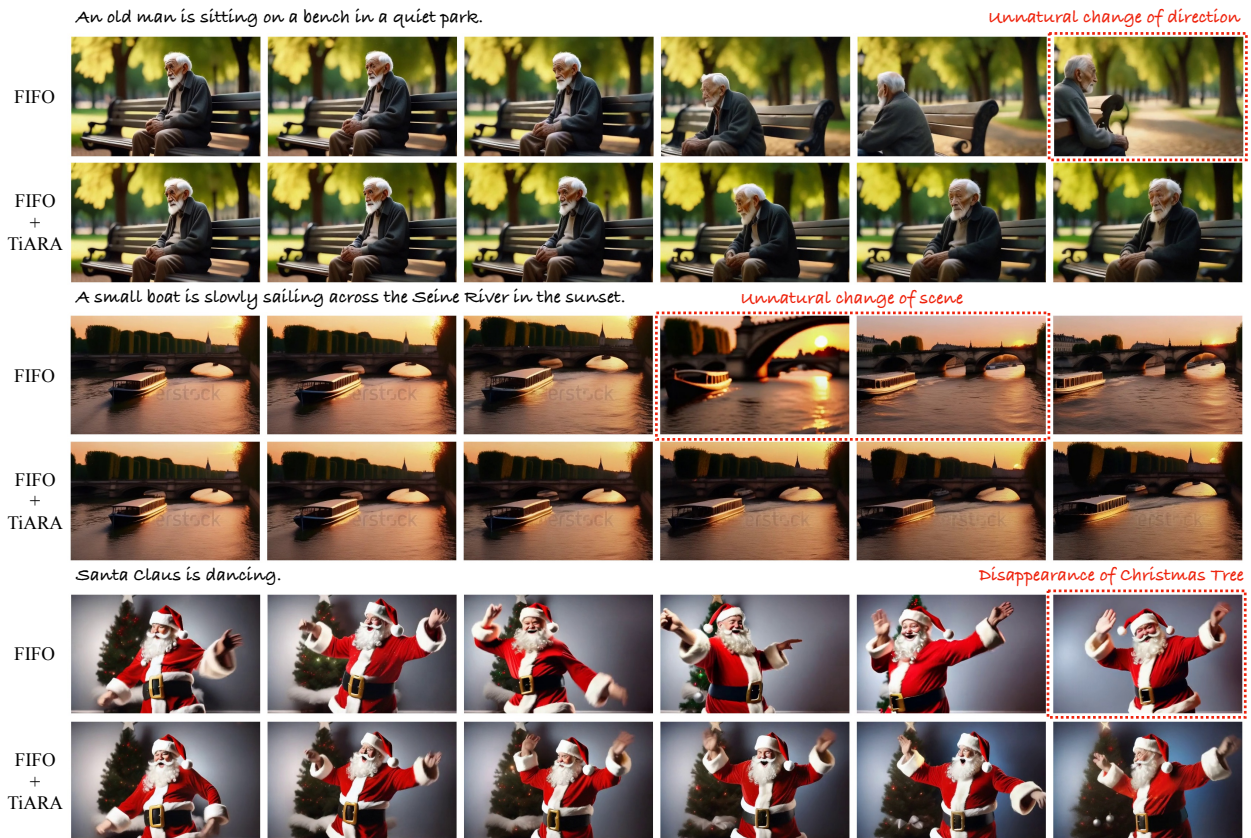


Figure 10: **Qualitative comparison on FIFO.** The first row of each example is the result with original FIFO; the second row is the result with FIFO augmented with TiARA. The displayed frames are sampled at fixed intervals. The inconsistent part in the videos are marked with red dotted boxes.

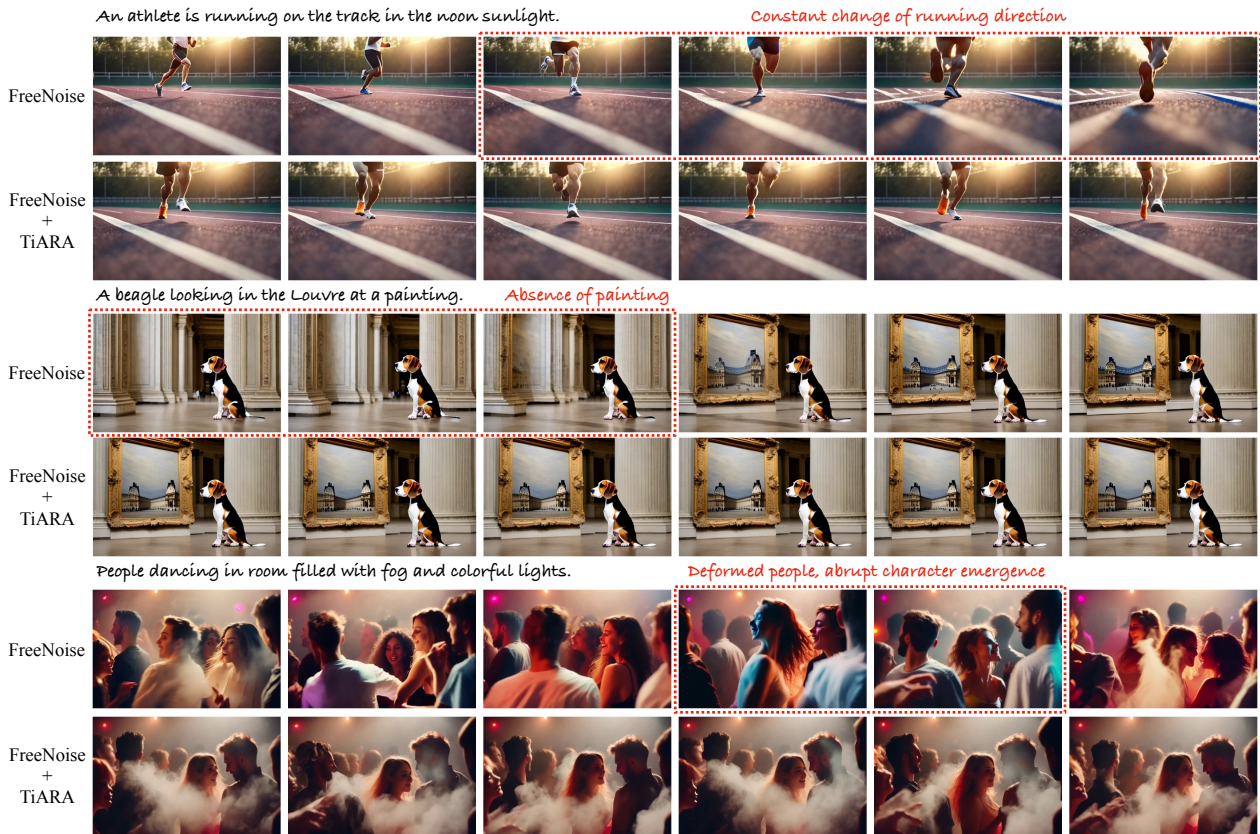


Figure 11: **Qualitative comparison on FreeNoise.** The first row of each example is the result with original FreeNoise; the second row is the result with FreeNoise augmented with TiARA. The displayed frames are sampled at fixed intervals. The inconsistent part in the videos are marked with red dotted boxes.

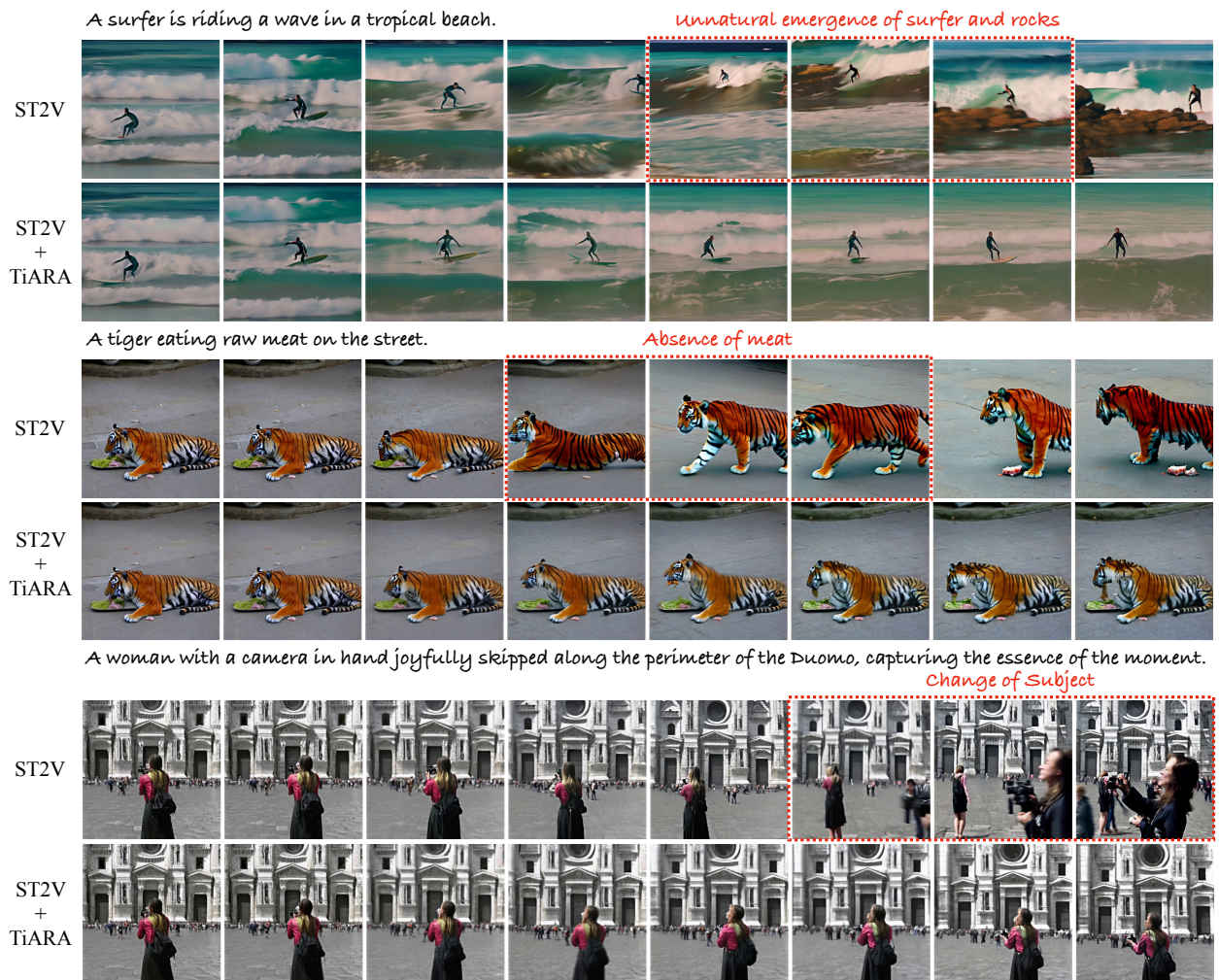


Figure 12: **Qualitative comparison on StreamingT2V (ST2V)**. The first row of each example is the result with original ST2V; the second row is the result with ST2V augmented with TiARA. The displayed frames are sampled at fixed intervals. The inconsistent part in the videos are marked with red dotted boxes.

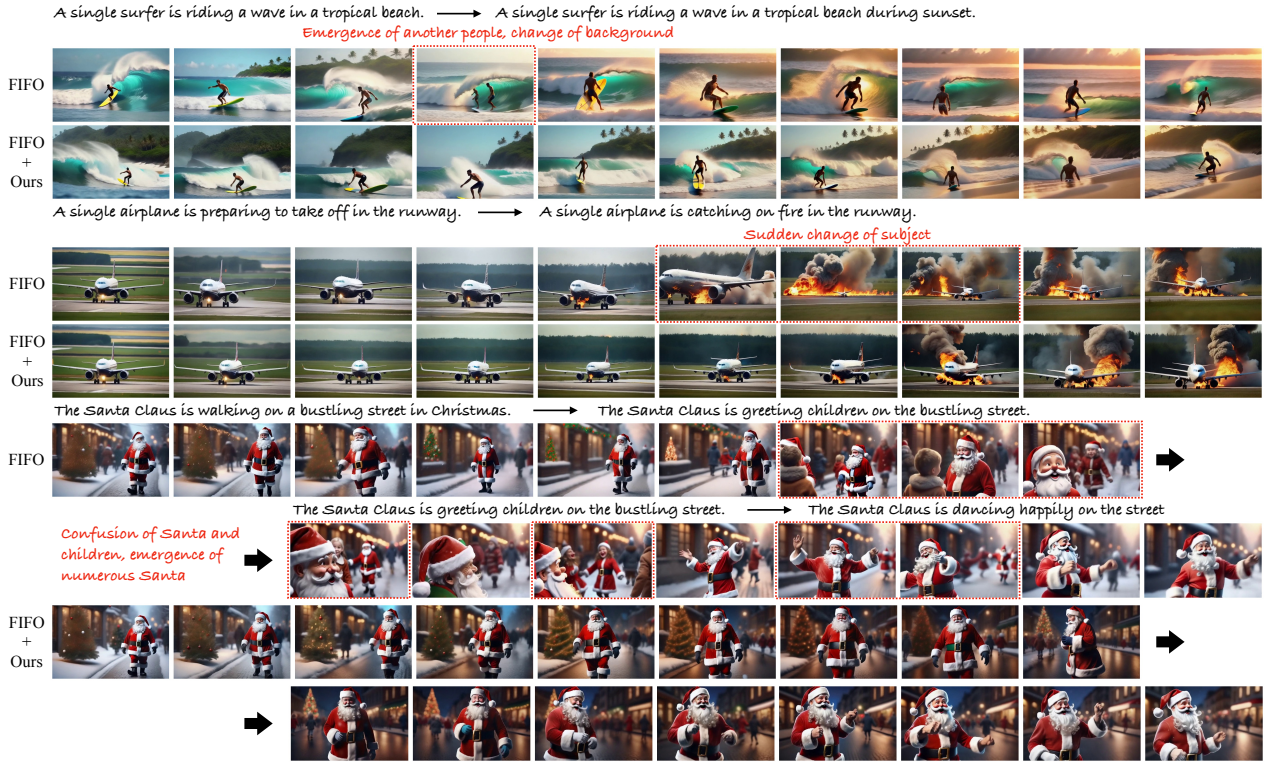


Figure 13: **Qualitative comparison on multi-prompt video generation.** The first two examples are generated with two prompts, and the third example is generated with three prompts. The first row of each example is the result with original multi-prompt FIFO; the second row is the result with FIFO + TIARA + PROMPTBLEND. The displayed frames are sampled at fixed intervals. The inconsistent part in the videos are marked with red dotted boxes.